Engineered Science

RESEARCH PAPER

View Article Online

Concerted Catalysis on *Tanghulu*-like Cu@Zeolitic Imidazolate Framework-8 (ZIF-8) Nanowires with Tuning Catalytic Performances for 4-nitrophenol Reduction

Dengfeng Wu,† Xing Zhang,† Jiqin Zhu and Daojian Cheng*

We report a facile strategy for the fabrication of *Tanghulu*-like Cu@ZIF-8 nanowires (NWs) by using poly(vinylpyrrolidone)-modified Cu NWs as seeds at normal temperature and pressure. The protecting and directing effects of poly(vinylpyrrolidone) (PVP) are crucial for the *in-situ* growth of ZIF-8 on Cu NWs. ZIF-8 particles are strung by Cu NW in single Cu@ZIF-8 NW. The catalytic performance of *Tanghulu*-like Cu@ZIF-8 NWs is much depended on the coverage of ZIF-8 due to the concerted catalysis, resulting in the tuning catalytic performances of beaded and core-shell structures. Particularly, the beaded Cu@ZIF-8 NWs exhibited significantly enhanced catalytic performance for the reduction of 4-nitrophenol (4-NP). ZIF-8 on Cu NWs can offer an enhanced capacity for adsorbing reactants (BH_4^- and 4-NP) and rapidly transfer active hydrogen species and 4-NP^- toward Cu active sites. This work offers a simple strategy for the architecture of other promising beaded one-dimensional structure as enhanced functional materials.

Keywords: Cu nanowires; ZIF-8; Beaded; Core-shell; 4-nitrophenol reduction

Received 9th May 2018, Accepted 21st May 2018

DOI: 10.30919/es8d718

1. Introduction

Developing effective, low-cost and environmental friendly nanocatalysts for the transformation of nitro compounds and water-soluble aromatic dyes to value products is crucial to human health and environmental sustainability.[1] 4-nitrophenol (4-NP), derived mainly from industrial and agricultural wastewater, is one of the most common and hazardous organic pollutant for its toxic, carcinogenic and biorefractory characters.[2–4] While, 4-NP is widely used as the precursor for production of 4-aminophenol (4-AP), which is less poisonous and used for photographic developer, corrosion inhibitor, drying agent, and also used as important intermediates in the preparation of analgesic and antipyretic drugs.[5–8] Hence, the catalytic reduction of 4-NP to 4-AP is of great significance for pollutant elimination and resources regeneration. Moreover, this reaction is also widely recognized as a trusted model reaction for assessing the catalytic properties of nanostructures.[8–10] Till now, great efforts have been focused on applying noble metal based nanocatalysts (Au, Ag, Pt, Pd) to catalyze the reduction of 4-NP by $NaBH_4$ to 4-AP.[11–18] Although those noble metal based catalysts display excellent catalytic activity, designing non-noble metal based catalysts with low cost, high activity and facile method are more desirable for future large-scale industrial applications.[19–29] Among these non-noble metal based catalysts, Cu-based catalysts exhibit impressive performances for 4-NP reduction.[25,30–32]

Recently, controllable integration of metallic nanocrystals (MNCs) and metal-organic frameworks (MOFs) into advanced materials has attracted a great deal of research attention for catalysis.[33–35] Particularly, MOFs can provide a tunable coordination space and chemical tailoring of the inner surface of the channels and cavities, which make them a promising new class of catalyst supports for hosting nanoparticles, especially for metallic MNCs in heterogeneous catalysis.[36–38] However, the MOFs-supported MNCs are still limited in catalytic performance because of the thermodynamic instability and aggregation of MNCs on the MOFs.[38,39] Therefore, encapsulating NCs into MOFs to form the MNCs@MOFs core-shell or core-shell-like nanostructures are considered to be one of the most promising ways to achieve synergies of metallic MNCs and MOFs.[37,40,41] Moreover, recent investigations have indicated that MOFs are promising participants for 4-NP reduction.[40,42,43] The stability and chemical activity of the MNC cores are preserved since the migration and aggregation of the NC cores can be dramatically limited by the MOF shells. However, for the catalytic process, although the MOFs are known as porous materials with ordered crystalline pores, the diffusion of the reactants or products between active sites on the surface of MNCs and bulk solution may be dragged down by the MOF shells, resulting into a mediocre catalytic performance. Therefore, a more striking way is

Beijing Key Laboratory of Energy Environmental Catalysis, State Key Laboratory of Organic-Inorganic Composites, Beijing University of Chemical Technology, Beijing 100029, China. E-mail: chengdj@mail.buct.edu.cn

† These authors contributed equally to this work.

to design and develop a new beaded structure with partially exposed and partially covered MNC core. Limited by the slenderness ratio, zero-dimensional nanostructure is hard to meet this requirement.

One dimensional metal NWs, such as Cu NWs, are attracting special interest due to their large slenderness ratio, anti-aggregating and high electron transport property.[44–46] Our previous studies indicate that Cu NW is a promising template for the preparation of one dimensional core-shell nanostructures.[47–50] In the series of MOFs, zeolitic imidazolate framework-8 (ZIF-8) as a kind of zeolitic imidazole-based MOF with large cavities interconnected by narrow windows has potential applications on target materials capturing and catalytic process.[51] Recently, Zhang and his co-workers reported that Cu NWs threaded ZIF-8 can be used as efficient catalysts for H_2 production from ammonia borane hydrolysis.[52] ZIF-8 on Cu NWs can offer a large capacity for adsorbing reactants and channels for rapidly transferring active hydrogen toward Cu active sites. Therefore, to architecture the optimized Cu NWs/ZIF-8 structures is a promising way to realize the highly efficient catalysis for 4-NP reduction in the presence of $NaBH_4$. A traditional Chinese snack called *Tanghulu*, sugarcoated haws on a stick, gives us inspiration.

Herein, *Tanghulu*-like Cu@ZIF-8 NWs are synthesized *via* a facile method by using PVP-modified Cu NWs as seeds at normal temperature and pressure. ZIF-8 particles are distributed individually and discontinuously along the axis of Cu NWs. Particularly, PVP plays a crucial role in the preparation of beaded Cu@ZIF-8 NWs since its directing and protecting effects. Moreover, the growth of ZIF-8 on Cu NWs can be well controlled from beaded to core-shell structures. Due to the synergetic catalysis of ZIF-8 and Cu NWs, the beaded Cu@ZIF-8 NWs exhibit significantly enhanced catalytic performance toward the reduction of 4-NP. The apparent reaction rate constant of beaded Cu@ZIF-8 NWs (0.0224 s^{-1}) is about 3-fold and 5-fold higher than that of Cu NWs (0.0083 s^{-1}) and core-shell Cu@ZIF-8 NWs (0.0043 s^{-1}). The enhanced mechanism of the reduction was proposed by using the Langmuir-Hinshelwood model.

2. Experimental section

2.1. Synthesis

2.1.1. Chemicals. Bis(acetylacetonato) copper(II) ($Cu(acac)_2$, 97%), Nickel chloride hexahydrate ($NiCl_2{\cdot}6H_2O$, > 98%), Dimethyl distearylammonium chloride ($C_{38}H_{80}ClN$, D1821, 97%), Poly(vinylpyrrolidone) (PVP, molecular weight of 24000, AR) and Oleylamine ($C_{18}H_{37}N$, 90%) were purchased from Aladdin. Zinc nitrate hydrate ($Zn(NO_3)_2{\cdot}xH_2O$, 98%), 2-Methylimidazole (2-MI, 98%), Sodium borohydride ($NaBH_4$), 4-nitrophenol were purchased from Maclin. Hexane (AR), acetone and methanol were purchased from Tianjin GuangFu Company. High pure nitrogen (N_2) was procured from Beijing RuYuanRuQuan Gas Company. All chemicals were used without further purification.

2.1.2. Synthesis of *Tanghulu*-like Cu@ZIF-8 NWs. Cu NWs were synthesized in advance according to a nonaqueous method derived from our previous work.[45,47] Typically, 0.8 mmol $Cu(acac)_2$, 0.4 mmol $NiCl_2{\cdot}6H_2O$ and 0.5 mmol D1821 were dissolved in 8 mL of oleylamine in a 50 mL three-neck flask and kept at 80 °C for 20 min under strong stirring in a N_2 stream. The temperature was then raised to 185 °C for 4 h. After the system cooled down to room temperature, Cu NWs were obtained by washing and centrifugation with sufficient hexane and acetone. The products were dispersed in methanol for standby application.

To prepare the *Tanghulu*-like Cu@ZIF-8 NWs, 1 g of PVP and 20 mg Cu NWs were dissolved in 125 mL methanol solution under magnetic stirring for 24 h. Then, the dispersion was centrifuged at 8000 rpm for 5 min and washed with methanol for three times. After that, 417.6 mg of $Zn(NO_3)_2{\cdot}6H_2O$ was added into 100 mL methanol with PVP-modified Cu NWs under magnetic stirring for another 60 min. Then, 20 mL methanol containing 116.5 mg 2-methylimidazole were also added into the above solution under magnetic stirring for 5 min or 15 min. All the above operations are completed under room temperature (25 °C) and normal pressure. Depending on the different reaction time, the products were named as "beaded Cu@ZIF-8 NWs" (5 min) and "core-shell Cu@ZIF-8 NWs" (15 min). The obtained products were separated via centrifugation at 8000 rpm for 5 min and further washed with methanol for several times. Subsequently, the product was vacuum-dried at 50 °C for 24 h.

2.2. Characterization

Structure and morphology of the catalysts were investigated using X-ray diffraction (XRD, D8 ADVANCE type (BRUKER-Germany)), transmission electron microscopy (TEM, Tecnai G2 F20 S-TWIN), scan electron microscopy (SEM, Hitachi S-4800), element mapping analysis (EDS mapping, JEOL JEM-2010) and high-angle annular dark field-scanning electron microscope (HAADF-STEM, JEOL JEM-2010). Elemental analyses were performed using inductively coupled plasma spectrometer (ICP, Thermo Scientific iCAP6000). Electronic environment of the catalysts were obtained by the X-ray photoelectron spectroscopy (XPS, Thermofisher ESCALAB 250). The N_2 adsorption-desorption isotherms were measured at 77 K using a Micromeritics ASAP 2046 instrument, from which, the specific surface area (S_{BET}) and pore volume (V_P) were calculated by applying Brunauer-Emmett-Teller (BET) and Barrett-Joyner-Halenda (BJH) models, respectively. The Fourier transform infrared (FTIR) spectroscopy studies were performed on a Nicolet 8700 FTIR spectrometer with the sample powders diluted in KBr pellets. The UV-vis absorption spectra were measured with a Puxi TU-1901 spectrophotometer.

2.3. Catalytic reduction of 4-NP

In a typical process, the catalytic reduction of 4-NP in the presence of $NaBH_4$ was carried out as follows. 0.7 mL of $NaBH_4$ (0.04 M, aqueous solution) was added 1.7 mL of 4-NP (0.1 mM, aqueous solution) as the reducing agent in a quartz cell (3 mL). Then, 30 μL of as-prepared catalyst suspension (15 mM, aqueous solution) was injected into the mixture of 4-NP and $NaBH_4$, and progress of the reaction were detected by a UV-vis spectrophotometer at different time intervals. The activation parameters for each reduction reaction were calculated. To examine the recyclability of self-synthesized catalysts, five cycles of the reduction of 4-NP were performed.

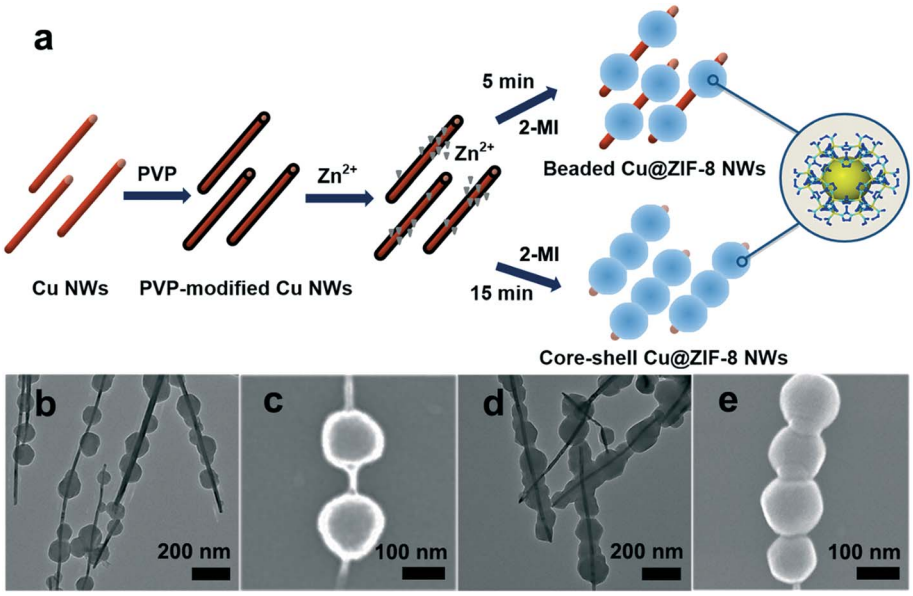

Fig. 1 (a) Schematic illustration of the synthesis of Cu@ZIF-8 NWs at room temperature. TEM and SEM images of (b, c) beaded and (d, e) core-shell structures.

3. Results and discussion

3.1. Synthesis and characterization of the *Tanghulu*-like Cu@ZIF-8 NWs

In the synthesis of *Tanghulu*-like Cu@ZIF-8 NWs (Figure 1a), the surfaces of Cu NWs are modified by PVP molecular chains at first, and then ZIF-8 particles are *in-situ* growth on the surface of PVP-modified Cu NWs by successively adding zinc salt and 2-MI into methanol medium. Since the ZIF-8 deposition on Cu NW can be well controlled by reaction time, two different Cu@ZIF-8 structures can be obtained (beaded and core-shell Cu@ZIF-8 NWs). The typical morphologies of these products were confirmed by TEM and SEM (Figure 1b-e). For beaded structures, Cu NWs are only partially encapsulated by ZIF-8 particles (Figure 1b and c). And ZIF-8 particles with average size of 127 nm (Figure S1a) are distributed discontinuously and strung by Cu NW with average diameter of 26 nm (Figure S1b). Moreover, Cu NWs are well retained after ZIF-8 deposition compared to the initial state (Figure S2a). Different to free particles (Figure S2b), ZIF-8 particles on Cu NWs are spherical rather than dodecahedral, which is in corresponding to other reports.[53,54] This should be attributed to the different nucleation processes in the formation of ZIF-8.[55,56] For core-shell structures (Figure 1d and e), ZIF-8 particles are end-to-end and totally encapsulate Cu NWs inside.

The elemental distribution of beaded Cu@ZIF-8 NWs and core-shell Cu@ZIF-8 NWs are checked by HAADF-STEM images and corresponding EDS elemental mapping of Cu, Zn, C and N, respectively. As shown in Figure 2a, the beaded structure with liner distribution of Cu and spherical distribution of Zn, C and N can be clearly observed, indicating that the beaded structure of Cu@ZIF-8 NWs is confirmed. Similarly, the core-shell Cu@ZIF-8 NWs are also confirmed by HAADF-STEM and EDS mapping analysis (Figure 2b).

In order to study the crucial of PVP in the controlling synthesis of *Tanghulu*-like Cu@ZIF-8 NWs, control experiments were conducted, and the products were characterized by TEM. The reactions in the absence of PVP could not yield Cu@ZIF-8 NWs (Figure 3a and b). In detail, only dodecahedral ZIF-8 particles with uneven size can be observed when the concentration of reactants (2-MI and Zn^{2+}) is high in reaction solution without PVP, indicating that Cu NWs were dissolved in the formation of ZIF-8 (Figure 3a). This result is in accordance with our previous work.[57] The dissolution of Cu NWs should be attributed to the deprotonation of 2-MI in the formation of ZIF-8,[58,59] and then the produced hydrogen protons can erosion the unprotected Cu NWs. The result infers that PVP can effectively protect Cu NWs free from dissolution. When the concentration of 2-methylimidazole and Zn^{2+} are reduced by half, the residual Cu NWs and sphere-like ZIF-8 particles are out of touch (Figure 3b), indicating that the ZIF-8 tends to self-seeding nucleation and growth without PVP on Cu NWs. Based on above results, it can be inferred that PVP modified layer can effectively protect the Cu NWs free of erosion by hydrogen protons and also serve as a guidance for the *in-situ* growth of ZIF-8 on Cu NWs rather than self-seeding nucleation (Figure 3c). Indispensably, careful cleaning is strongly necessary since the PVP layer on the surface of Cu NWs may seriously hinder the subsequent catalytic performances.

As shown in Figure 4a, XRD measurements were performed to examine the crystalline phase of *Tanghulu*-like Cu@ZIF-8 NWs. Cu

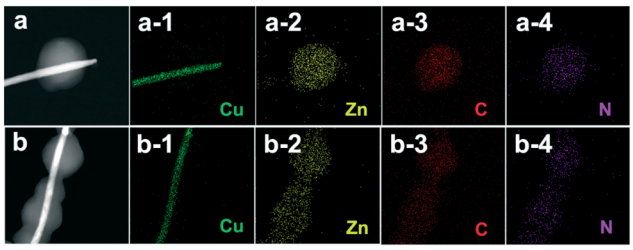

Fig. 2 (a) HAADF-STEM image of beaded Cu@ZIF-8 NWs and corresponding EDS elements mapping of (a-1) Cu, (a-2) Zn, (a-3) C and (a-4) N. (b) HAADF-STEM image of core-shell Cu@ZIF-8 NWs and corresponding EDS elements mapping of (b-1) Cu, (b-2) Zn, (b-3) C and (b-4) N.

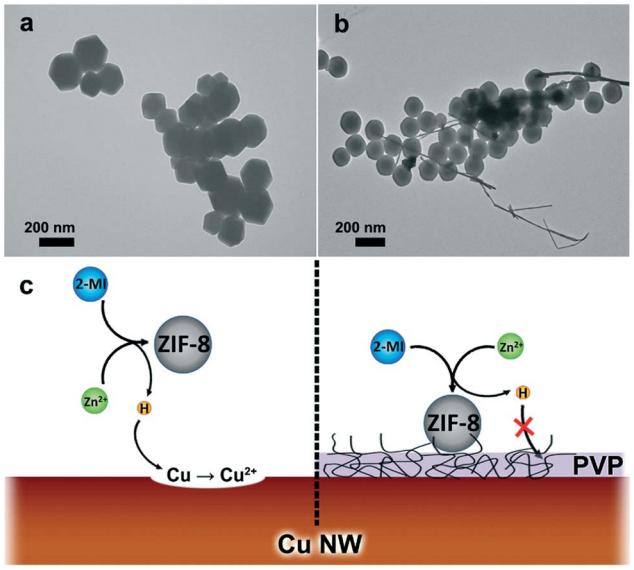

Fig. 3 TEM images of the products obtained in reaction solution with (a) high and (b) low concentration of reactants (2-methylimidazole and Zn^{2+}) in the absence of PVP. (c) Schematic illustration of the directing and protecting effect of PVP on Cu NWs.

NWs and free ZIF-8 particles are also exhibited for comparison. For beaded or core-shell Cu@ZIF-8 NWs, peaks appear at 43.3°, 50.4°, 74.1° should be assigned to the (111), (200), and (220) faces of pure Cu (JCPDS PDF#04-0836) with face-centered cubic (fcc) structure. In addition to the diffraction peaks of Cu phase, the other diffraction peaks should be assigned to ZIF-8 phase, which is corresponding to the previous work.[60] The results indicate that the obtained Cu@ZIF-8 NWs are composed of two independent and stable phases including Cu and ZIF-8. Information on surface chemistry of bare Cu NWs, beaded and core-shell Cu@ZIF-8 NWs were investigated by XPS analysis (Figure 4b). For beaded or core-shell structures, Cu 2p, Zn 2p, C 1s, N 1s and O 1s peaks can be observed on the curves, in which Cu 2p peaks should be attributed to the Cu NWs while Zn 2p, C 1s, N 1s and O 1s peaks should be attributed to the ZIF-8 particles. It is found that Cu 2p signal peaks for bare Cu NWs are much stronger than those for Cu@ZIF-8 NWs (insert in Figure 4b). Moreover, the Cu signal peaks become weaker and weaker with the increment of ZIF-8 deposition, indicating that the different nude degree of Cu NWs for Cu@ZIF-8 NWs. The XPS results suggest that the beaded or core-shell structures are further confirmed.

As shown in Figure 4c, free ZIF-8 particles, beaded and core-shell Cu@ZIF-8 NWs display a similar type of N_2 adsorption-desorption isotherm and pore-size-distribution curves. It is found that the BET surface area (S_{BET}) of the beaded Cu@ZIF-8 NWs can reach up to 668 m^2/g and the corresponding pore volume (V_P) is 0.282 cm^3/g (Table 1). However, the S_{BET} and V_P of beaded Cu@ZIF-8 NWs is much lower than that of pure ZIF-8 (1555 m^2/g, 0.653 cm^3/g) or core-shell Cu@ZIF-8 NWs (806 m^2/g, 0.353 cm^3/g), suggesting that the S_{BET} and V_P of the composites are much depended on ZIF-8 content or Cu content, which could be expressed as Cu wt. % determined by ICP analysis. As shown in the pore-size distribution analysis (Figure 4d), the incorporation of Cu NWs does not alter the pore-size distribution of ZIF-8 (1~2 nm), indicating that the Cu NWs do not occupy the porous channels in ZIF-8. The enlarged BET surface area and single aperture distribution can offer a large capacity for adsorbing reactants and channels for rapidly transferring small molecules (e.g. hydrogen species) toward Cu active sites.[61] While, the uncovered Cu could provide more efficient active sites for characteristic reaction than that of covered one.[62]

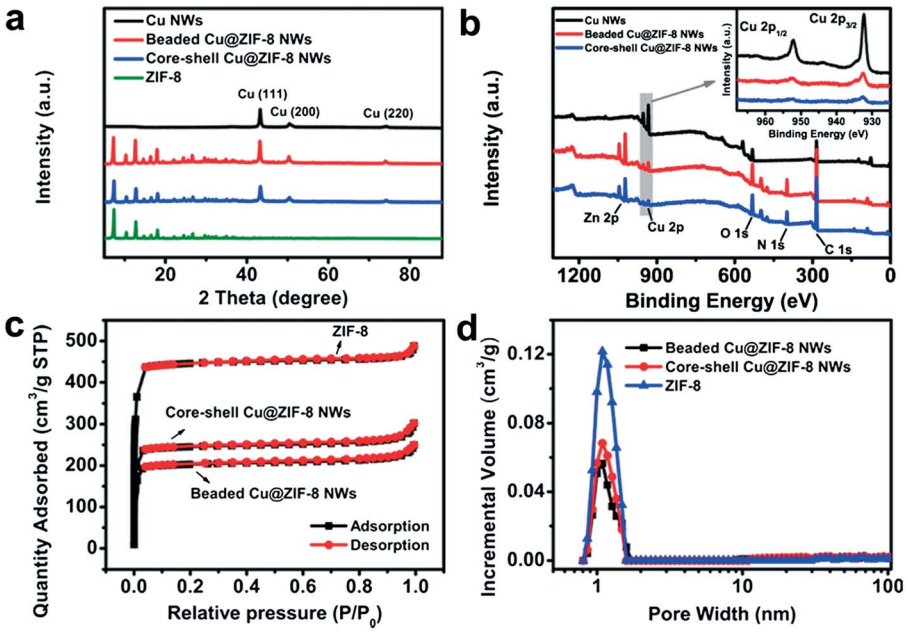

Fig. 4 (a) XRD patterns of beaded Cu@ZIF-8 NWs, Cu NWs, free ZIF-8 particles and core-shell Cu@ZIF-8 NWs. (b) The XPS spectrum of Cu NWs, beaded Cu@ZIF-8 NWs and the core-shell Cu@ZIF-8 NWs. (c) N_2 adsorption-desorption isotherms of beaded Cu@ZIF-8 nanowires, core-shell Cu@ZIF-8 nanowires and ZIF-8 and (d) pore-size-distribution curves obtained from the desorption data through the BJH method.

Table 1 Specific surface area (S_{BET}), pore volumes (V_P), Cu quality fraction (Cu wt. %) and active factor (k_{nor}) of beaded Cu@ZIF-8 NWs, core-shell Cu@ZIF-8 NWs, ZIF-8 and Cu NWs.

Catalyst	S_{BET} (m^2 g^{-1})	V_P (cm^3 g^{-1})	Cu wt. %	k_{nor} (s^{-1} mg^{-1})
Beaded Cu@ZIF-8 NWs	668	0.282	39.06	1.9912
Core-shell Cu@ZIF-8 NWs	806	0.353	35.97	0.4151
ZIF-8	1555	0.653	--	--
Cu NWs	--	--	95.91	0.3005

Note: Cu wt. % was determined by ICP.

3.2. Catalytic reduction of 4-NP

The catalytic reduction of 4-NP to 4-AP on self-synthesized catalysts was carried out at normal temperature and pressure. The UV-vis absorption spectra of the reaction solution was analyzed to investigate the reduction process. Aqueous 4-NP shows a absorption peak at 317 nm (Figure 5a). While, upon the addition of $NaBH_4$, the alkalinity of the solution increased and 4-nitrophenolate ions ($4\text{-}NP^-$) would become the dominating species,[63,64] along with a spectral shift of the absorption peak to 400 nm. The color of solution changes from light yellow to dark yellow (insert in Figure 5a). Without additional

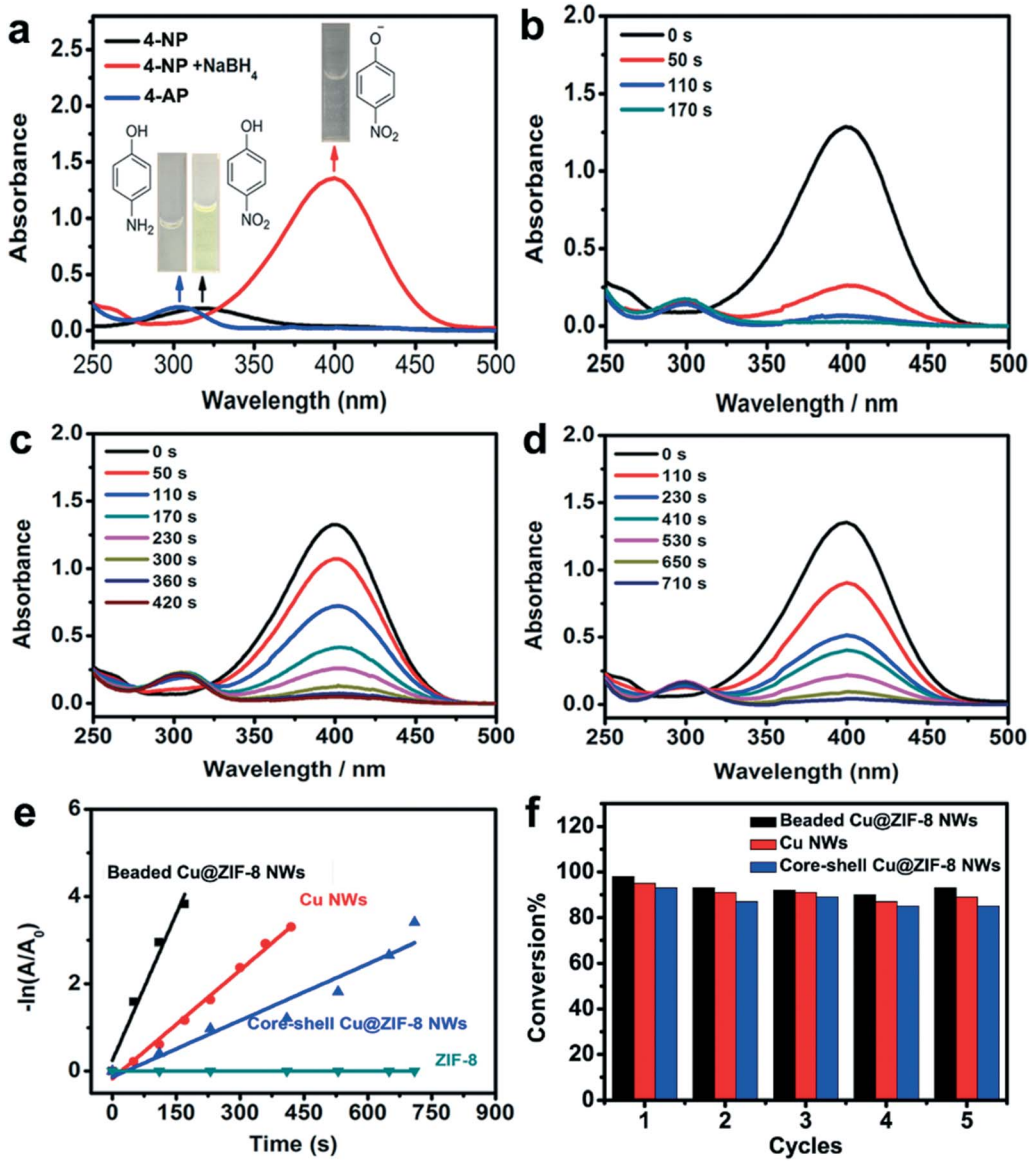

Fig. 5 (a) UV-Vis absorption spectra about 4-NP, upon the addition of $NaBH_4$ and 4-NP. Time-dependent UV-Vis absorption spectra upon the addition of (b) beaded Cu@ZIF-8 NWs, (c) Cu NWs and (d) core-shell Cu@ZIF-8 NWs. (e) Plots of $-\ln(A/A_0)$ against the reaction time for the reduction of 4-NP catalyzed by different catalysts. (f) Recyclability of beaded Cu@ZIF-8 NWs, Cu NWs and core-shell Cu@ZIF-8 NWs.

catalysts, the mixture will stay yellow and the maximum absorption peak will remain unaltered, suggesting that the reduction would not be proceeded without catalysts.

As shown in Figure 5b, when a small amount of beaded Cu@ZIF-8 NWs are added to the mixture, the absorption peak at 400 nm drops sharply as the reduction reaction proceeded. Simultaneously, a new absorption peak starts is uprising at 300 nm with the production of 4-AP. Moreover, the UV-vis spectra show an isosbestic point between the two absorption bands, indicating that the 4-NP is gradually converted to 4-AP without side reaction.[65] After 170 s, the absorption peak centered at 400 nm is disappeared completely, suggesting that the reduction process is finished. Then the color of solution changes from dark yellow to colorless (insert in Figure 5a). For comparison, the catalytic performances of bare Cu NWs and core-shell Cu@ZIF-8 NWs were investigated under the same conditions. However, the reaction time on Cu NWs and core-shell Cu@ZIF-8 NWs is 420 s and 710 s respectively (Figure 5c-d), which is much longer than that of beaded Cu@ZIF-8 NWs, indicating the enhanced performance of beaded Cu@ZIF-8 NWs. Figure 5e shows the relationship between the depletion of the 400 nm peak and reaction time by measuring the recorded UV-vis absorption (i.e., $\ln(C/C_0)$ vs. reduction time), suggesting that the reaction is a pseudo-first order.[66] We use the regression of the slope from the logarithm plot ($-dC_t/dt = k_{app}C_t$) estimate the activity factor (k_{app}). The k_{app} value of the beaded Cu@ZIF-8 NWs is 0.0224 s^{-1}, which is about 3-fold and 5-fold higher than that of Cu NWs (0.0083 s^{-1}) and the core-shell Cu@ZIF-8 NWs (0.0043 s^{-1}), respectively, evidencing the enhanced catalytic performance of the beaded Cu@ZIF-8 NWs. Moreover, for comparing our result with other catalysts in previous investigations, the activity factors were normalized by the loading of catalyst ($k_{nor} = k_{app}/m$). Herein, Cu loading of catalyst were demonstrated by ICP analysis. It is found that the k_{nor} value of beaded Cu@ZIF-8 NWs is larger than that of most of previous Cu-based catalysts or other noble catalysts (Table S1), indicating that the beaded Cu@ZIF-8 NWs is an excellent catalyst for 4-NP reduction. In addition, recyclability is also critical for the practical application of a catalyst. Generally, conversion is an important parameter to evaluate the recyclability of a catalyst.[24] To examine the recyclability of beaded Cu@ZIF-8 NWs, Cu NWs and core-shell Cu@ZIF-8 NWs, five cycles of the reduction of 4-NP were performed (Figure 5f). After five catalytic cycles, the conversion of the beaded Cu@ZIF-8 NWs is still as high as 93% and decreases only by 5%, which is smaller than that of Cu NWs (6%) and core-shell Cu@ZIF-8 NWs (8%). Recyclability results indicate that the beaded Cu@ZIF-8 NWs may be a promising catalyst for efficient 4-NP reduction.

According to the previous studies and above results, the whole process can be described by following equations.[67–69]

$BH_4^- + 2H_2O \rightarrow BO_2^- +$ actives hydrogen species

4-NP $\rightarrow$ 4-NP^-

4-NP^- + actives hydrogen species $\rightarrow$ 4-AP

The adsorbed active hydrogen species from the hydrolysis of $NaBH_4$ and 4-NP^- from the deprotonation of 4-NP are crucial intermediates in the hydrogenation process. Figure 6a shows the hydrogen evolution profile by using ZIF-8 and Cu NWs as catalysts, respectively. It is found that the hydrogen evolution performance of ZIF-8 particles is much better than that of Cu NWs, indicating that the main active sites for the hydrolysis of $NaBH_4$ are mainly on ZIF-8 particles. For the beaded Cu@ZIF-8 NWs, the porous ZIF-8 particles can serve as reservoirs and provided transport channels for active hydrogen species toward bare Cu active sites. Concurrently, 4-NP^- would also be formed on the surface of catalysts. Figure 6b shows the UV-Vis absorption spectra of 4-NP transformation with different catalysts in absence of $NaBH_4$. It is found that the absorption peak shifts completely from 317 to 400 nm in presence of ZIF-8. However, for Cu NWs, the absorption peak at 317 nm is going down, but still remains some residual. And the absorption peak shifts partially in presence of Cu NWs, indicating that the ZIF-8 is a more efficient catalyst than Cu NWs for the transformation of 4-NP to 4-NP^-. Although ZIF-8 is an efficient catalysts for $NaBH_4$ hydrolysis and 4-NP transformation, it has no catalytic activity for the 4-NP^- reduction to 4-AP (Figure 5e), indicating that Cu NWs served as the active sites for the last step of reaction. Therefore, it can be inferred that the efficient catalytic process is based on the concerted catalysis of ZIF-8 and Cu NWs.

Based on above results, the possible enhanced mechanism of 4-NP reduction on beaded Cu@ZIF-8 was proposed (Figure 7). Firstly, ZIF-8 on Cu NWs could accelerate the adsorption of BH_4^- and 4-NP. Since the differences of kinetic diameters (Figure S3), BH_4^- can penetrate into ZIF-8, while 4-NP can only be absorbed on the surface of ZIF-8.[38] Secondly, a large number of intermediates (active hydrogen species and 4-NP^-) will be produced by ZIF-8, resulting in the formation of a high concentration of the reaction intermediates around the bared Cu NWs relative to bulk solution. According to the Langmuir-Hinshelwood (LH) model,[8,69] the

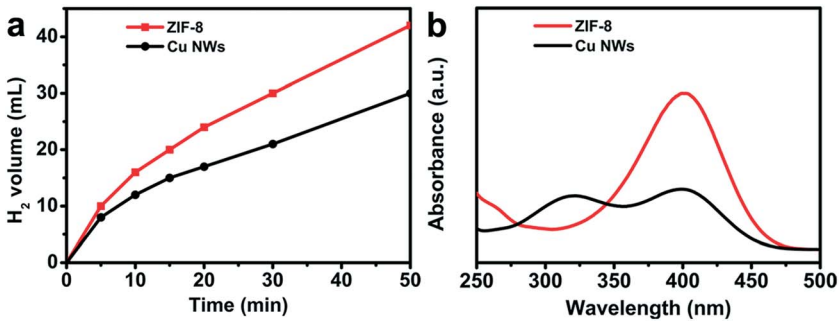

Fig. 6 (a) Catalytic hydrogen generation performances of ZIF-8 and Cu NWs from sodium borohydride hydrolysis reaction. (b) UV-Vis absorption spectra of 4-NP transformation upon the addition of the different catalysts.

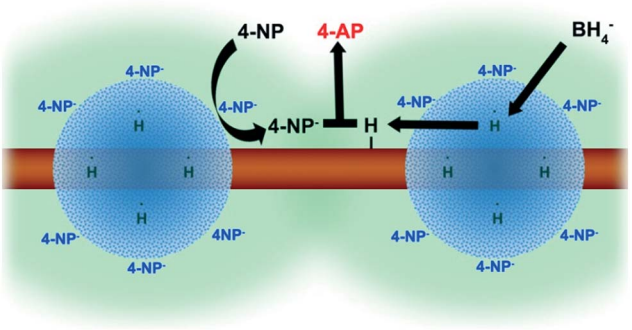

Fig. 7 Proposed mechanism for the reduction of 4-NP to 4-AP in the presence of $NaBH_4$ on beaded Cu@ZIF-8 NWs.

hydrogenation process will happen between the co-adsorbed active hydrogen species and 4-NP^- on Cu NWs. Finally, 4-AP desorbs from the surface of the catalysts. In addition, a positive shift of 0.12 eV for Cu $2P_{3/2}$ of *Tanghulu*-like Cu@ZIF-8 NWs was observed compared to that of the bare Cu NWs (932.40 eV) as shown in the XPS result (insert in Figure 4b), indicating that a strong interaction was formed between Cu NWs and ZIF-8. Such interactions could be favorable for accelerating the transfer of dissociated active hydrogen species from ZIF-8 to Cu NWs.[52] Moreover, the electronic structure changes of Cu may also improve the intrinsic reactivity of catalysts. For core-shell Cu@ZIF-8 NWs, the inferior performance should be attributed to the blocked last step of reaction.

4. Conclusions

In summary, *Tanghulu*-like Cu@ZIF-8 NWs have been synthesized *via* a facile method by using PVP-modified Cu NWs as seeds at room temperature. ZIF-8 particles are distributed discontinuously along the axis of Cu NWs. Particularly, PVP plays a crucial role in the preparation of beaded Cu@ZIF-8 NWs since its directing and protecting effects. Moreover, the growth of ZIF-8 on Cu NWs can be well controlled from beaded to core-shell structures. Due to the synergetic catalysis of ZIF-8 and Cu NWs, the beaded Cu@ZIF-8 NWs (0.0224 s^{-1}) exhibit much better performance to give apparent reaction rate constants about 3-fold and 5-fold higher than Cu NWs (0.0083 s^{-1}) and the as-synthesized core-shell Cu@ZIF-8 NWs (0.0043 s^{-1}). This work opens up a simple strategy for the architecture of other promising beaded one-dimensional structure as enhanced functional materials.

Conflict of interest

There are no conflicts to declare.

Acknowledgments

This work is supported by the National Natural Science Foundation of China (21576008, 91634116, 91334203), the Fundamental Research Funds for the Central Universities (PYCC1705) and PetroChina Innovation Foundation (2016D-5007-0505).

References

1 M. T. Amin, A. A. Alazba and U. Manzoor, *Adv. Mater. Sci. Eng.*, 2014, **2014**, 24.
2 J. Li, D. Kuang, Y. Feng, F. Zhang, Z. Xu and M. Liu, *J. Hazard. Mater.*, 2012, **201**, 250–259.
3 J. Zhang, G. Chen, D. Guay, M. Chaker and D. Ma, *Nanoscale*, 2014, **6**, 2125–2130.
4 J.-G. You, C. Shanmugam, Y.-W. Liu, C.-J. Yu and W.-L. Tseng, *J. Hazard. Mater.*, 2017, **324**, 420–427.
5 H. Hu, J. H. Xin and H. Hu, *J. Mater. Chem. A*, 2014, **2**, 11319–11333.
6 M. Guo, J. He, Y. Li, S. Ma and X. Sun, *J. Hazard. Mater.*, 2016, **310**, 89–97.
7 L. Lunar, D. Sicilia, S. Rubio, D. Pérez-Bendito and U. Nickel, *Water Res.*, 2000, **34**, 1791–1802.
8 P. Zhao, X. Feng, D. Huang, G. Yang and D. Astruc, *Coordin. Chem. Rev.*, 2015, **287**, 114–136.
9 P. Herves, M. Perez-Lorenzo, L. M. Liz-Marzan, J. Dzubiella, Y. Lu and M. Ballauff, *Chem. Soc. Rev.*, 2012, **41**, 5577–5587.
10 S. Zhang, S. Gai, F. He, Y. Dai, P. Gao, L. Li, Y. Chen and P. Yang, *Nanoscale*, 2014, **6**, 7025–7032.
11 Y.-C. Chang and D.-H. Chen, *J. Hazard. Mater.*, 2009, **165**, 664–669.
12 W. Shen, Y. Qu, X. Pei, S. Li, S. You, J. Wang, Z. Zhang and J. Zhou, *J. Hazard. Mater.*, 2017, **321**, 299–306.
13 W. Zhang, F. Tan, W. Wang, X. Qiu, X. Qiao and J. Chen, *J. Hazard. Mater.*, 2012, **217**, 36–42.
14 J. Li, J. Liu, Y. Yang and D. Qin, *J. Am. Chem. Soc.*, 2015, **137**, 7039–7042.
15 X. Lin, M. Wu, D. Wu, S. Kuga, T. Endo and Y. Huang, *Green Chem.*, 2011, **13**, 283–287.
16 S. K. Srivastava, M. Guix and O. G. Schmidt, *Nano Lett.*, 2016, **16**, 817–821.
17 L. Liu, R. Chen, W. Liu, J. Wu and D. Gao, *J. Hazard. Mater.*, 2016, **320**, 96–104.
18 A. T. E. Vilian, S. R. Choe, K. Giribabu, S.-C. Jang, C. Roh, Y. S. Huh and Y.-K. Han, *J. Hazard. Mater.*, 2017, **333**, 54–62.
19 G. Wu, X. Liang, L. Zhang, Z. Tang, M. Al-Mamun, H. Zhao and X. Su, *ACS Appl. Mater. Interfaces*, 2017, **9**, 18207–18214.
20 C. Wang, L. Salmon, R. Ciganda, L. Yate, S. Moya, J. Ruiz and D. Astruc, *Chem. Commun.*, 2017, **53**, 644–646.
21 L. Dou, Y. Wang, Y. Li and H. Zhang, *Dalton Trans.*, 2017, **46**, 15836–15847.
22 B.M. Mogudi, P. Ncube, N. Bingwa, N. Mawila, S. Mathebula and R. Meijboom, *Appl. Catal. B-Environ.*, 2017, **218**, 240–248.
23 H. Chen, M. Yang, S. Tao and G. Chen, *Appl. Catal. B-Environ.*, 2017, **209**, 648–656.
24 X. Huang, D. Wu and D. Cheng, *J. Colloid. Interface Sci.*, 2017, **507**, 429–436.
25 J. Jiang, Y. Soo Lim, S. Park, S. -H. Kim, S. Yoon and L. Piao, *Nanoscale*, 2017, **9**, 3873–3880.
26 D. Zhang, G. Zhang and L. Zhang, *Chem. Eng. J.*, 2017, **330**, 792–803.
27 L. Zhang, Y. Li, Q. Zhang and H. Wang, *CrystEngComm*, 2013, **15**, 5986–5993.
28 Z. Li, L. Yaogang, Z. Qinghong, S. Guoying and W. Hongzhi, *Chem. Lett.*, 2011, **40**, 1371–1373.
29 L. Zhang, Y. Li, H. Xie, H. Wang and Q. Zhang, *J. Nanosci. Nanotechno.*, 2015, **15**, 2944.
30 Z.-Y. Xiao, S.-R. Zhai, X.-P. Ma, Z. -Y. Zhao, X. Wang, H. Bai and Q.-D. An, *New J. Chem.*, 2017, **41**, 13230–13234.
31 C. Huang, W. Ye, Q. Liu and X. Qiu, *ACS Appl. Mater. Interfaces*, 2014, **6**, 14469–14476.
32 B. Dinesh and R. Saraswathi, *Sensor. Actuat. B-Chem.*, 2017, **253**, 502–512.
33 Q. Yang, Q. Xu and H.-L. Jiang, *Chem. Soc. Rev.*, 2017, **46**, 4774–4808.
34 L. An, L. Huang, P. Zhou, J. Yin, H. Liu and P. Xi, *Adv. Func. Mater.*, 2015, **25**, 6814–6822.
35 T. T. Dang, Y. Zhu, J. S. Y. Ngiam, S. C. Ghosh, A. Chen and A. M. Seayad, *ACS Catal.*, 2013, **3**, 1406–1410.
36 H.-L. Jiang, T. Akita, T. Ishida, M. Haruta and Q. Xu, *J. Am. Chem. Soc.*, 2011, **133**, 1304–1306.
37 M. Zhao, K. Deng, L. He, Y. Liu, G. Li, H. Zhao and Z. Tang, *J. Am. Chem. Soc.*, 2014, **136**, 1738–1741.
38 S. Li and F. Huo, *Small*, 2014, **10**, 4371–4378.
39 R. Senthil Kumar, S. Senthil Kumar and M. Anbu Kulandainathan, *Micropor. Mesopor. Mater.*, 2013, **168**, 57–64.
40 C. Wang, H. Zhang, C. Feng, S. Gao, N. Shang and Z. Wang, *Catal. Commun.*, 2015, **72**, 29–32.

41 Q. Yang, Q. Xu, S.-H. Yu and H.-L. Jiang, *Angew. Chem. Int. Ed.*, 2016, **55**, 3685–3689.
42 J. Li, F. Wu, L. Lin, Y. Guo, H. Liu and X. Zhang, *Chem. Eng. J.*, 2018, **333**, 146–152.
43 Z. Hasan, D.-W. Cho, C.-M. Chon, K. Yoon and H. Song, *Chem. Eng. J.*, 2016, **298**, 183–190.
44 A. K. Patra, A. Dutta and A. Bhaumik, *Catal. Commun.*, 2010, **11**, 651–655.
45 B. Chen, D. Cheng and J. Zhu, *J. Power Sources*, 2014, **267**, 380–387.
46 D. Zhang, R. Wang, M. Wen, D. Weng, X. Cui, J. Sun, H. Li and Y. Lu, *J. Am. Chem. Soc.*, 2012, **134**, 14283–14286.
47 D. Wu, H. Xu, D. Cao, A. Fisher, Y. Gao and D. Cheng, *Nanotechnology*, 2016, **27**, 495403.
48 S. Li, D. Cheng, X. Qiu and D. Cao, *Electrochim. Acta*, 2014, **143**, 44–48.
49 D. Cheng, D. Wu, H. Xu and A. Fisher, *ChemistrySelect*, 2016, **1**, 4392–4396.
50 D. Wu, W. Zhang and D. Cheng, *ACS Appl. Mater. Interfaces*, 2017, **9**, 19843–19851.
51 J. Yao and H. Wang, *Chem. Soc. Rev.*, 2014, **43**, 4470–4493.
52 D. Zhang, P. Liu, S. Xiao, X. Qian, H. Zhang, M. Wen, Y. Kuwahara, K. Mori, H. Li and H. Yamashita, *Nanoscale*, 2016, **8**, 7749–7754.
53 Y. Pan, Y. Liu, G. Zeng, L. Zhao and Z. Lai, *Chem. Commun.*, 2011, **47**, 2071–2073.
54 N. L. Torad, M. Hu, Y. Kamachi, K. Takai, M. Imura, M. Naito and Y. Yamauchi, *Chem. Commun.*, 2013, **49**, 2521–2523.
55 H.-L. Jiang, B. Liu, T. Akita, M. Haruta, H. Sakurai and Q. Xu, *J. Am. Chem. Soc.*, 2009, **131**, 11302–11303.
56 X. Liu, L. He, J. Zheng, J. Guo, F. Bi, X. Ma, K. Zhao, Y. Liu, R. Song and Z. Tang, *Adv. Mater.*, 2015, **27**, 3273–3277.
57 H. Yu, A. Fisher, D. Cheng and D. Cao, *ACS Appl. Mater. Interfaces*, 2016, **8**, 21431–21439.
58 S. Tanaka, T. Nagaoka, A. Yasuyoshi, Y. Hasegawa and J.F.M. Denayer, *Cryst. Growth. Des.*, 2018, **18**, 274–279.
59 K. Kida, M. Okita, K. Fujita, S. Tanaka and Y. Miyake, *CrystEngComm*, 2013, **15**, 1794–1801.
60 M. He, J. Yao, Q. Liu, K. Wang, F. Chen and H. Wang, *Micropor. Mesopor. Mater.*, 2014, **184**, 55–60.
61 P.-Z. Li, K. Aranishi and Q. Xu, *Chem. Commun.*, 2012, **48**, 3173–3175.
62 P. Zhang, Y. Sui, G. Xiao, Y. Wang, C. Wang, B. Liu, G. Zou and B. Zou, *J. Mater. Chem. A*, 2013, **1**, 1632–1638.
63 M. Li and G. Chen, *Nanoscale*, 2013, **5**, 11919–11927.
64 J. Pal, C. Mondal, A. K. Sasmal, M. Ganguly, Y. Negishi and T. Pal, *ACS Appl. Mater. Interfaces*, 2014, **6**, 9173–9184.
65 N. Pradhan, A. Pal and T. Pal, *Colloid. Surface. A*, 2002, **196**, 247–257.
66 K.-L. Wu, X.-W. Wei, X.-M. Zhou, D.-H. Wu, X.-W. Liu, Y. Ye and Q. Wang, *J. Phys. Chem. C*, 2011, **115**, 16268–16274.
67 S. Bae, S. Gim, H. Kim and K. Hanna, *Appl. Catal. B-Environ.*, 2016, **182**, 541–549.
68 J. Huang, S. Vongehr, S. Tang, H. Lu and X. Meng, *J. Phys. Chem. C*, 2010, **114**, 15005–15010.
69 S. Wunder, F. Polzer, Y. Lu, Y. Mei and M. Ballauff, *J. Phys. Chem. C*, 2010, **114**, 8814–8820.

